

# SCIENTIFIC REPORTS



OPEN

## Selectivity Mechanism of the Voltage-gated Proton Channel, $H_{V1}$

Received: 23 February 2015

Accepted: 08 April 2015

Published: 08 May 2015

Todor Dudev<sup>1,2</sup>, Boris Musset<sup>3</sup>, Deri Morgan<sup>4</sup>, Vladimir V. Cherny<sup>4</sup>, Susan M. E. Smith<sup>5</sup>, Karine Mazmanian<sup>1,6</sup>, Thomas E. DeCoursey<sup>4</sup> & Carmay Lim<sup>1,7</sup>

Voltage-gated proton channels,  $H_{V1}$ , trigger bioluminescence in dinoflagellates, enable calcification in coccolithophores, and play multifarious roles in human health. Because the proton concentration is minuscule, exquisite selectivity for protons over other ions is critical to  $H_{V1}$  function. The selectivity of the open  $H_{V1}$  channel requires an aspartate near an arginine in the selectivity filter (SF), a narrow region that dictates proton selectivity, but the mechanism of proton selectivity is unknown. Here we use a reduced quantum model to elucidate how the Asp–Arg SF selects protons but excludes other ions. Attached to a ring scaffold, the Asp and Arg side chains formed bidentate hydrogen bonds that occlude the pore. Introducing  $H_3O^+$  protonated the SF, breaking the Asp–Arg linkage and opening the conduction pathway, whereas  $Na^+$  or  $Cl^-$  was trapped by the SF residue of opposite charge, leaving the linkage intact, thus preventing permeation. An Asp–Lys SF behaved like the Asp–Arg one and was experimentally verified to be proton-selective, as predicted. Hence, interacting acidic and basic residues form favorable  $AspH^0-H_2O^0-Arg^+$  interactions with hydronium but unfavorable  $Asp^-X^-/X^+-Arg^+$  interactions with anions/cations. This proposed mechanism may apply to other proton-selective molecules engaged in bioenergetics, homeostasis, and signaling.

The voltage-gated proton channel,  $H_{V1}$ , has been implicated in numerous biological functions in humans<sup>1</sup>: charge compensation during the respiratory burst of phagocytes killing bacteria<sup>2,3</sup>, pH homeostasis in airway epithelia<sup>4</sup>, histamine secretion by basophils<sup>5</sup>, and triggering sperm capacitation<sup>6</sup>. It is a desirable and novel drug target<sup>7</sup> due to its involvement in various inflammatory pathologies and its exacerbation of diseases such as ischemic stroke<sup>8</sup>, breast cancer<sup>9</sup>, and chronic lymphocytic leukemia<sup>10</sup>. In other species  $H_{V1}$  channels play diverse roles including mediating action potentials that trigger bioluminescence in dinoflagellates<sup>11</sup> and enabling biogenic calcite production by coccolithophores as part of the global carbon cycle<sup>12</sup>. The ability of  $H_{V1}$  to perform its functions would fail if its proton selectivity were not perfect, due to the low concentration of protons in biological fluids. A conserved aspartate (Asp112 in humans) in the middle of the S1 transmembrane helix is an essential part of the  $H_{V1}$  selectivity filter (SF)<sup>11,13</sup>. This Asp consistently interacts with the second<sup>14,15</sup> or third<sup>16,17</sup> Arg in the S4 segment in homology models of human  $H_{V1}$  (h $H_{V1}$ ) in an open (proton-conducting) conformation. However, it is seen to interact with the second Arg in the crystal structure of a closely related voltage-sensing phosphatase in the active conformation<sup>18</sup>. Classical molecular dynamics (MD) simulations indicate that charge compensation (e.g., an intact salt bridge) appears essential<sup>19</sup>, but do not reveal the mechanism by which proton selectivity

<sup>1</sup>Institute of Biomedical Sciences, Academia Sinica, Taipei 115, Taiwan. <sup>2</sup>Faculty of Chemistry and Pharmacy, Sofia University, Sofia 1164, Bulgaria. <sup>3</sup>Institute of Complex Systems (ICS-4 Zelluläre Biophysik), Forschungszentrum Jülich, Jülich, NRW, Germany. <sup>4</sup>Department of Molecular Biophysics and Physiology, Rush University, Chicago, IL 60612, USA. <sup>5</sup>Department of Biology and Physics, Kennesaw State University, Kennesaw, GA 30144, USA. <sup>6</sup>Chemical Biology and Molecular Biophysics Program, Taiwan International Graduate Program, Academia Sinica, Nankang, Taipei 11529, Taiwan. <sup>7</sup>Department of Chemistry, National Tsing Hua University, Hsinchu 300, Taiwan. Correspondence and requests for materials should be addressed to T.E.D. (email: tdecours@rush.edu) or C.L. (email: carmay@gate.sinica.edu.tw)

occurs. Might selectivity result from obligatory protonation and deprotonation of a titratable group<sup>13,20</sup> lining the SF? How does an Asp in a constricted SF select protons, while rejecting other cations/anions?

Takeshita *et al.*<sup>21</sup> have determined a 3.45 Å structure of a chimeric murine H<sub>V</sub>1 channel in a probable closed conformation. This structure shows that the SF Asp is located in a hydrophobic layer comprising two conserved Phe residues, which might prevent water penetration. Presumably, this hydrophobic region prevents conduction of any ions including protons in closed channels. We adopt the nearly universal assumption that channel opening involves a protein conformational change. Opening allows H<sub>3</sub>O<sup>+</sup> to access the SF from either side of the membrane. Since no 3D structure of H<sub>V</sub>1 in an open conformation has been solved, hypotheses on proton selectivity and conduction have been based on homology models derived from the open-state structures of voltage-gated sodium or potassium channels, which share only 13–19% sequence identity with hH<sub>V</sub>1<sup>22</sup>. MD simulations of hH<sub>V</sub>1 using as templates the open-state structures of the K<sub>v</sub>AP (1ORS)<sup>23</sup> and the K<sub>v</sub>1.2-K<sub>v</sub>2.1 paddle chimera (2R9R)<sup>16</sup> potassium channels predict a stable water wire in the open channel. It is widely accepted that protons can be conducted efficiently along a hydrogen-bonded water chain<sup>24–28</sup>. However, MD simulations of the same hH<sub>V</sub>1 channel derived from multiple templates (1ORS, 2R9R, and 3RVY)<sup>14</sup> show that the Asp–Arg interaction, which interrupts the water wire, is only occasionally broken, yielding a transient water wire. Likewise, in simulations of *Ciona intestinalis* H<sub>V</sub>1<sup>17</sup>, which is homologous to hH<sub>V</sub>1 with 52% sequence identity, the average lifetime of a continuous water wire in an open-state model was only 6 ps. An ephemeral water-wire is suggestive of proton permeation involving titratable residues.

Whether proton selectivity could result from protonation/deprotonation of a titratable group can be answered only by considering explicit protonation/deprotonation reactions using all-electron quantum mechanical calculations, as done here. The lack of an open, proton-bound X-ray structure of hH<sub>V</sub>1 prohibits accurate evaluations of multi-ion free energy profiles for ion permeation. Thus, we evaluated selectivity by comparing the binding affinity of H<sub>3</sub>O<sup>+</sup>, Na<sup>+</sup>, Cl<sup>−</sup>, and H<sub>2</sub>O in the SF, assuming that the hH<sub>V</sub>1 would be selective to the permeating ion that binds with higher affinity in the SF. A reduced SF model was devised to capture the essential chemical processes underlying proton selectivity. It was designed to maximize resemblance to the open H<sub>V</sub>1 SF and was constructed on the basis of the following considerations: At the narrowest, relatively dry region of the pore<sup>14</sup>, the SF is lined by an aspartate (Asp112 in hH<sub>V</sub>1), which is conserved in all known and putative H<sub>V</sub>1. This Asp interacts almost continuously with one of the three Arg residues in the S4 transmembrane segment in the open channel from MD simulations based on different homology models<sup>14–17,29</sup>. Even when the Asp was moved by double mutation from position 112 to 116 (D112V/V116D), it still interacted with one or two Arg residues with an intact or a broken salt-bridge in MD simulations<sup>19</sup>. Intriguingly, a positive point charge pulled through this double mutant in the broken configuration encountered a 10 kcal/mol barrier, but no barrier in the intact salt-bridge configuration<sup>19</sup>. These findings indicate that the Asp–Arg interaction is essential to proton selectivity, hence it was incorporated into the SF model. Ions such as Na<sup>+</sup>, OH<sup>−</sup>, and Cl<sup>−</sup> were assumed to be dehydrated since the SF pore is purported to be narrow<sup>14,21</sup>. Ions in bulk solution were not included in the SF model, since H<sub>V</sub>1 channels are notoriously indifferent to ionic strength<sup>13</sup>, cations such as Ca<sup>2+</sup> or Mg<sup>2+</sup><sup>30,31</sup>, or anion species<sup>31</sup>.

To address whether proton selectivity arises from protonation and deprotonation of a titratable group, the interactions between the permeating ions and H<sub>V</sub>1 SF ligands, which play a key role in the competition between the native proton and its rivals, were treated explicitly using density functional theory to account for electronic effects such as polarization of the participating entities and differential amounts of ligand → ion charge transfer, while the region inside the SF was represented by a continuum dielectric. The proton was modeled as H<sub>3</sub>O<sup>+</sup>, while the Asp<sup>−</sup>, Arg<sup>+</sup>, Ala, His, and Lys<sup>+</sup> side chains were modeled as  $-\text{CH}_2\text{-COO}^-$ ,  $-\text{CH}_2\text{-NH-C}(\text{NH}_2)_2^+$ ,  $-\text{CH}_2\text{-CH}_3$ ,  $-\text{CH}_2\text{-imidazole}$ , and  $-\text{CH}_2\text{-NH}_3^+$ , respectively. The SF ligands were attached to a ring scaffold (see **Methods**), and the resulting complex was subject to all-electron geometry optimization without any constraints. The fully optimized SF geometries were then used to compute the ion-binding/exchange reactions in the H<sub>V</sub>1 pore characterized by an effective dielectric constant,  $\epsilon$ . Since MD simulations of the open-state hH<sub>V</sub>1 model<sup>14</sup> show that the SF is *not* in a bulk water environment but is relatively dry (see above), we employed  $\epsilon$  ranging from 4 to 30<sup>32</sup> to reflect a solvent-inaccessible or a partially solvent-exposed binding site, respectively, in order to encompass the actual value in the SF (see **Methods**). In interpreting results, we focus *not* on the absolute free energies, but on the change in ion-binding/exchange free energies with increasing  $\epsilon$ . The approach outlined above has yielded structures and free energy trends in model SFs of various ion channels that are consistent with experimental findings<sup>32–36</sup>. The distance found here between the charge centers of the SF Asp and Arg (3.7 Å) agrees with that (3.8–4.6 Å) in MD simulations of the open hH<sub>V</sub>1<sup>14,19</sup>. The free energy trends in the model H<sub>V</sub>1 SF found herein are also consistent with experimental findings.

## Results

**Binding of H<sub>3</sub>O<sup>+</sup> in the Asp–Arg SF.** The ion-free Asp–Arg SF adopted two closed conformations that differ by <1 kcal/mol: an ion-pair conformation where the Asp and Arg side chains formed a bidentate salt bridge (Fig. 1a) and a hydrogen-bonded pair conformation where Arg protonated Asp, forming two hydrogen bonds (Fig. 1b). An Arg-carboxylate structural motif identified in several enzymes is thought to ensure rapid equilibrium between protonated and deprotonated Arg<sup>37</sup>. To see how the SF could accommodate passing ions, H<sub>3</sub>O<sup>+</sup> was placed between Asp and Arg, above the hydrogen-bond

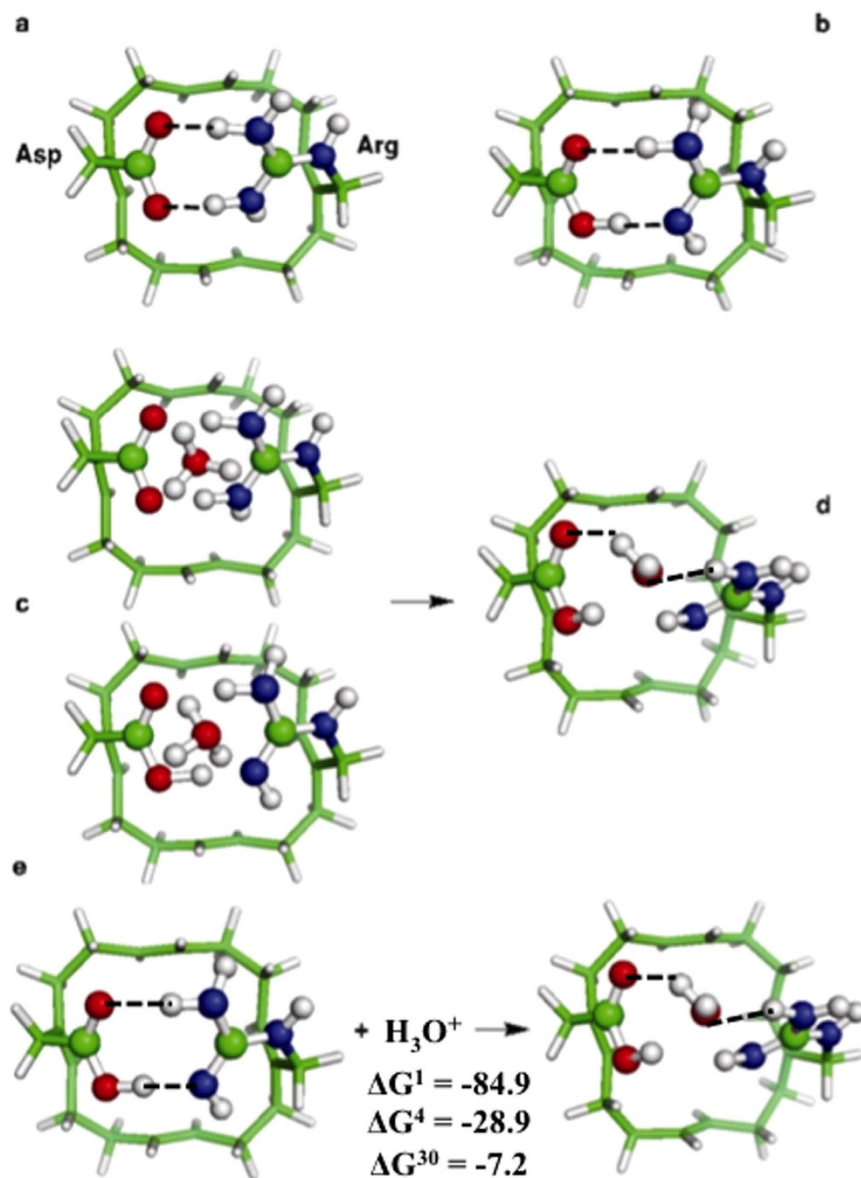


**Figure 1.** Binding of  $\text{H}_3\text{O}^+$  to the Asp-Arg SF. Fully optimized B3-LYP/6-31+G(3d,p) structures of (a) ion-free  $\text{Asp}^-$ - $\text{Arg}^+$  SF, (b)  $\text{Asp}^0$ - $\text{Arg}^0$  SF, (c) initial configurations of the SF- $\text{H}_3\text{O}^+$  complex and (d) final configuration of the SF- $\text{H}_3\text{O}^+$  complex,  $\text{AspH}^0$ - $\text{H}_2\text{O}$ - $\text{Arg}^+$  with H in grey, C in green, N in blue and O in red. A dashed line denotes a hydrogen bond, which is defined by a donor-acceptor distance  $\leq 3.5$  Å and a H-acceptor distance  $\leq 2.5$  Å. The reaction between SF and  $\text{H}_3\text{O}^+$  is depicted in (e) with free energies given in kcal/mol;  $\Delta G^1$  is the binding free energy in the gas phase, whereas  $\Delta G^4$  and  $\Delta G^{30}$  are the corresponding free energies in the SF characterized by an effective dielectric constant of 4 and 30, respectively.

network plane (Fig. 1c), mimicking the transient breaking of the Asp-Arg linkages, allowing  $\text{H}_3\text{O}^+$  into the SF. The positioning of  $\text{H}_3\text{O}^+$  between a deprotonated acid and a base has been observed spectroscopically<sup>38</sup>. In the final, fully optimized structure (Fig. 1d), the Asp and Arg side chains moved apart, breaking the two hydrogen bonds, thus opening the permeation pathway to accommodate the permeating  $\text{H}_3\text{O}^+$ , which transferred a proton to the SF leaving a water bridging  $\text{AspH}^0$  and  $\text{Arg}^+$ . Binding of  $\text{H}_3\text{O}^+$  to the Asp-Arg SF is thermodynamically favorable throughout the range of dielectric constant explored (negative  $\Delta G^x$ , Fig. 1e).

**Binding of  $\text{Cl}^-$  and  $\text{Na}^+$  to the Asp-Arg SF.** The Asp-Arg SF responded quite differently to the introduction of the proton's competitors,  $\text{Cl}^-$  and  $\text{Na}^+$ . We started from the “open” pore structure, where the Asp and Arg side chains were separated, and placed the incoming ion between them (Fig. 2, left). Such a configuration was not favorable as during geometry optimization, the introduced ion was ejected from the pore, away from the residue bearing the same charge and became trapped by the residue

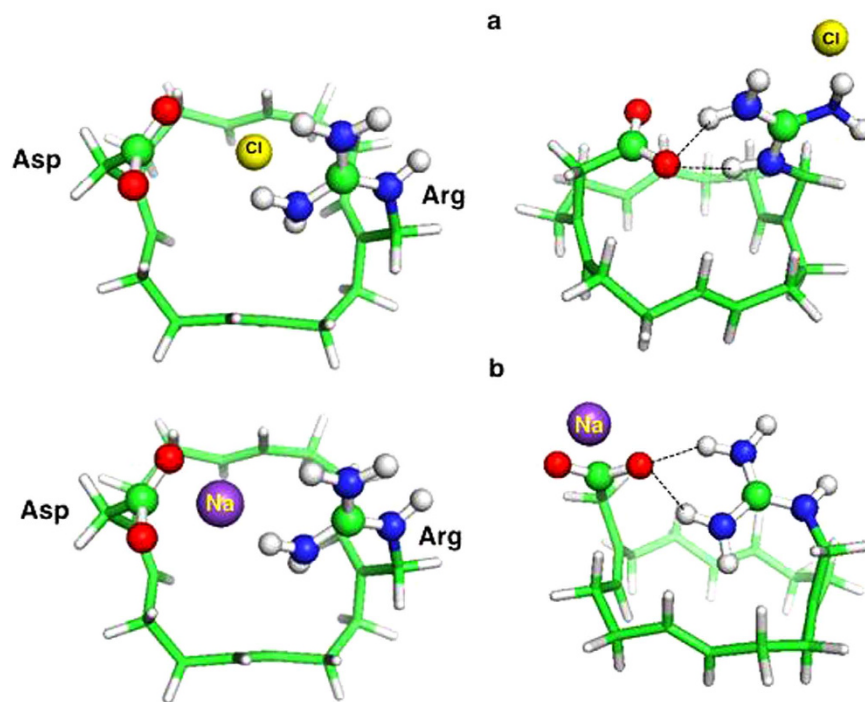


**Figure 2.** Binding of  $\text{Cl}^-$  and  $\text{Na}^+$  to Asp–Arg SF. Ball and stick diagrams of the initial (left) and final (right) structures of SF complexes with (a)  $\text{Cl}^-$  and (b)  $\text{Na}^+$ .

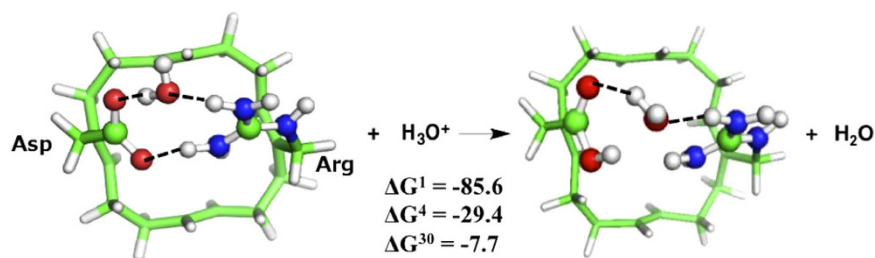


**Figure 3.** Free energies (in kcal/mol) for replacing  $\text{H}_2\text{O}$  bound in Asp–Arg SF with  $\text{H}_3\text{O}^+$ . See Fig. 1 legend.

carrying the opposite charge:  $\text{Arg}^+$  for  $\text{Cl}^-$  and  $\text{Asp}^-$  for  $\text{Na}^+$  (Fig. 2, right). In contrast to the open starting structures, the hydrogen-bond network between Asp and Arg was partially restored in the final optimized structures, closing the SF aperture and excluding other ions.

The above results highlight the importance for proton selectivity of electrostatic interactions between the SF and permeating ions. The SF Asp–Arg pair intrinsically selects protons and rejects other cations and anions: the only species that can bind favorably to both  $\text{Asp}^-$  and  $\text{Arg}^+$  in an “open” state is  $\text{H}_3\text{O}^+$  (Fig. 1e).  $\text{Cl}^-$  and  $\text{Na}^+$  are not permeable, as they do not promote pore opening (Fig. 2).

**$\text{H}_2\text{O}$  vs.  $\text{H}_3\text{O}^+$  Binding in the Asp–Arg SF.** Although the Asp112–Arg208 pair is broken only 10% of the time in MD simulations of a homology model of hH<sub>v</sub>1 in an open conformation, this transient disruption allows formation of a water wire that could last for 1 ns<sup>14</sup>. Would a water molecule be even more stable than  $\text{H}_3\text{O}^+$  in the H<sub>v</sub>1 SF? In other words, can  $\text{H}_3\text{O}^+$  displace water bound to the Asp–Arg pair? To address this question, we placed  $\text{H}_2\text{O}$  in between the Asp–Arg pair and optimized the structure. The fully optimized structure in Fig. 3 (left) shows that a water molecule, unlike  $\text{H}_3\text{O}^+$ , cannot fully dissociate the Asp–Arg pair, as a hydrogen bond remains between the two residues. Furthermore,  $\text{H}_3\text{O}^+$  can easily displace water bound to the Asp–Arg pair and protonate Asp (Fig. 3, right): The computed free energies ( $\Delta G^x$ ,  $x = 1-30$ ) for  $\text{H}_3\text{O}^+$  to displace  $\text{H}_2\text{O}$  from the Asp–Arg pair are all favorable (negative  $\Delta G^x$ , Fig. 3). The positive free energies for the reverse reaction imply that a water molecule cannot readily displace  $\text{H}_3\text{O}^+$  bound to the Asp–Arg pair.

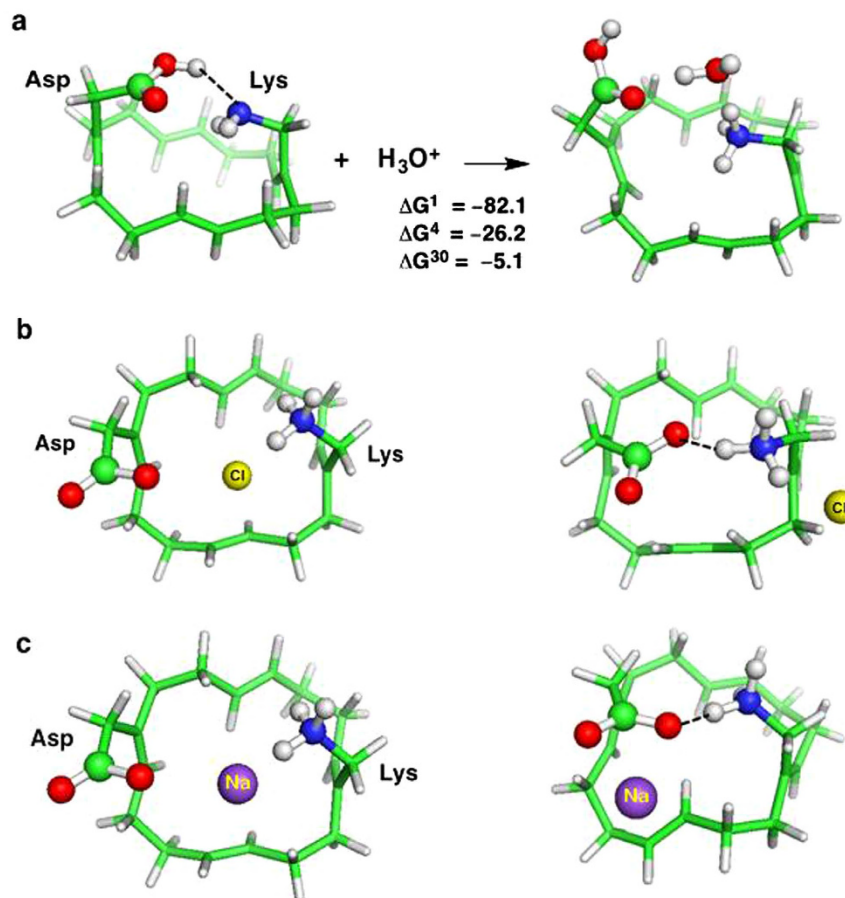


**Figure 4.** (a) Free energies (in kcal/mol) for binding of H<sub>3</sub>O<sup>+</sup> to Lys mutant SF. Ball and stick diagrams of the initial (left) and final (right) structures of Arg→Lys mutant SF complexes with Cl<sup>-</sup> (b) and Na<sup>+</sup> (c). See Fig. 1 legend.

**The Arg208Lys Mutant is Predicted to be Proton-selective.** Replacing the Lys lining the pore of voltage-gated Na<sup>+</sup> channels with Arg nearly abolishes the channel's selectivity for Na<sup>+</sup> over K<sup>+</sup><sup>39</sup>. Is Arg in the H<sub>v</sub>1 SF likewise indispensable for proton selectivity? To address this question, we replaced the SF Arg by Lys and evaluated its proton selectivity. Lys behaved like its Arg counterpart: in the ion-free state, Lys protonated Asp forming a hydrogen bond (Fig. 4a, left); however, because Lys has a lower pK<sub>a</sub> than Arg, a stable Asp<sup>-</sup>-Lys<sup>+</sup> ion pair minimum could not be found. In the ion-bound state, H<sub>3</sub>O<sup>+</sup>, which was initially placed between the protonated Asp and neutral Lys, transferred a proton to the SF leaving a water molecule to bridge AspH<sup>0</sup> and Lys<sup>+</sup> (Fig. 4a, right). The AspH<sup>0</sup>-H<sub>2</sub>O-Lys<sup>+</sup> complex formation free energies remain thermodynamically favorable, although slightly less so than those for the wild-type Asp-Arg SF (compare numbers in Figs. 1e and 4a). As in the wild-type SF, during geometry optimization, Cl<sup>-</sup> and Na<sup>+</sup> were repelled by the SF residue of the same net charge and moved towards the SF residue with the opposite charge. In the final optimized structures, Asp<sup>-</sup> and Lys<sup>+</sup> formed a hydrogen bond, prohibiting the competing Cl<sup>-</sup> and Na<sup>+</sup> ions from passing through the pore (Figs. 4b and 4c).

The prediction that the Lys mutant SF is selective for protons over other competing ions was verified experimentally by mutating Arg208 lining the SF to Lys: currents through the Lys208 mutant reversed near the Nernst potential for H<sup>+</sup> (Fig. 5); the reversal potential ( $V_{rev}$ ) did not change when Na<sup>+</sup> or K<sup>+</sup> replaced TMA<sup>+</sup> or Cl<sup>-</sup> replaced CH<sub>3</sub>SO<sub>3</sub><sup>-</sup> (Supplementary Table S5).

**Why D112A and D112H Mutants are Chloride-selective.** Mutagenesis studies<sup>13</sup> show that replacing Asp112 in the SF with a neutral residue such as Ala or the weak base His converts the channel into an anion-selective pore. Why? To address this question we modeled two types of SF mutants: Ala<sup>0</sup>-Arg<sup>+</sup> (Fig. 6a,b) and His<sup>0</sup>-Arg<sup>+</sup> (Fig. 6c). Replacing anionic Asp112<sup>-</sup> with neutral Ala or His leaves the positive charge on the SF Arg<sup>+</sup> uncompensated, which disfavors H<sub>3</sub>O<sup>+</sup> binding to the SF due to the like charge repulsion between H<sub>3</sub>O<sup>+</sup> and Arg<sup>+</sup>. On the other hand, strong attractive forces between the permeating OH<sup>-</sup>/Cl<sup>-</sup> and Arg<sup>+</sup> stabilize the OH<sup>-</sup>/Cl<sup>-</sup>-SF complexes, and thus favor binding of the anion. To verify that the Ala112 and His112 mutants would be anion-selective, we computed the free energy for replacing H<sub>3</sub>O<sup>+</sup> in the mutant SFs with Cl<sup>-</sup>. In line with the experimental observations, the Ala<sup>0</sup>-Arg<sup>+</sup> SF is

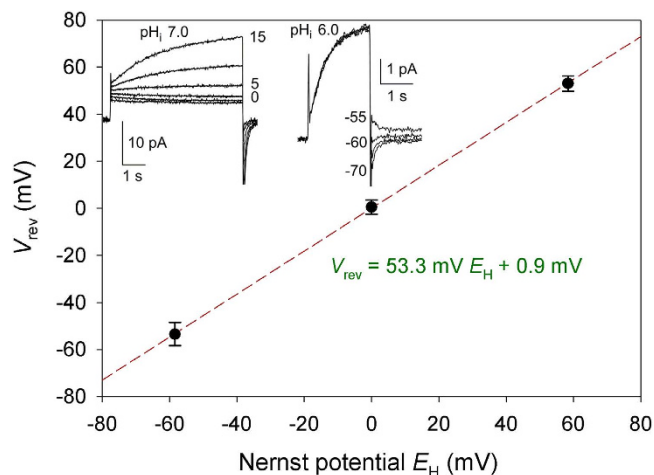


**Figure 5.** The Lys208 mutant is proton selective. Measured values of  $V_{\text{rev}}$  at  $\Delta\text{pH} -1.0, 0, \text{ or } 1.0$  (mean  $\pm$  SEM,  $n = 3, 9, \text{ or } 6$ , respectively), with  $\text{pH}_0$  ranging 5.5 to 7.0 and  $\text{pH}_i$  ranging 5.5 to 8.0. The linear regression slope was 53.3 mV/unit  $\Delta\text{pH}$ , compared with the Nernst value of 58.4 mV. *Inset:* Proton currents in an inside out patch during pulses applied in 5 mV increments (left) indicate reversal between 0 and 5 mV (the conductance activated negative to  $V_{\text{rev}}$ ) at  $\text{pH}_i 7.0$ , with  $\text{pH}_0 7.0$  (in the pipette). Tail currents in the same patch at  $\text{pH}_i 6.0$  indicate reversal at  $-58$  mV. Both values are near the Nernst predictions of 0 mV and  $-58.4$  mV.

highly  $\text{Cl}^-$ -selective in both solvent-inaccessible and exposed pores (negative  $\Delta G^x$ , Fig. 6a). It is predicted to be even more selective for  $\text{OH}^-$  (more negative  $\Delta G^x$  in Fig. 6b than in Fig. 6a), in accord with the experimental finding that the Asp112Ala mutant is more permeable to  $\text{OH}^-$  than to  $\text{Cl}^-$ <sup>13</sup>. This is likely so because the SF Arg can protonate  $\text{OH}^-$ , yielding a neutral  $\text{Ala}^0\text{-H}_2\text{O}^0\text{-Arg}^0$  complex.

Like the  $\text{Ala}^0\text{-Arg}^+$  mutant, the  $\text{His}^0\text{-Arg}^+$  SF is predicted to be also anion-selective provided the narrow pore has limited solvent accessibility (negative  $\Delta G^4$ ), which is seen in the 3.45 Å crystal structure of a mouse  $\text{H}_V1$  chimeric channel (PDB 3WKV)<sup>21</sup> and in simulations of open-state  $\text{H}_V1$  models<sup>14,17</sup>. However, it is predicted to be less  $\text{Cl}^-$ -selective than the  $\text{Ala}^0\text{-Arg}^+$  filter (less negative  $\Delta G^4$  in Fig. 6c than in Fig. 6a), which is also consistent with experiment<sup>13</sup>. This is largely because  $\text{H}_3\text{O}^+$  protonated the His-Arg SF, stabilizing the  $\text{His}^+\text{-H}_2\text{O}\text{-Arg}^+$  “reactant” complex (Fig. 6c, left), but no such stabilization can occur in the  $\text{Ala}^0\text{-H}_3\text{O}^+\text{-Arg}^+$  “reactant” complex (Fig. 6a, left).

## Discussion

Previous studies<sup>16,23</sup> have proposed that a water wire might conduct protons through  $\text{H}_V1$ , but this does not explain how other ions are excluded and why an aspartate (Asp112 in humans) in the  $\text{H}_V1$  pore is essential for proton selectivity<sup>11,13</sup>. This work shows that the  $\text{H}_V1$  Asp-Arg SF selects protons by transferring a proton from  $\text{H}_3\text{O}^+$  to the SF, highlighting the importance of quantum effects (charge transfer and polarization). Although a water molecule can be inserted between Asp and Arg, it is readily displaced by  $\text{H}_3\text{O}^+$  (Fig. 3), which then transfers its extra proton to the SF.

This work suggests the following proton selectivity mechanism in the  $\text{H}_V1$  SF: On a time-scale of seconds, the channel helices, S4 in particular<sup>18,40</sup>, move from a closed conformation that does not allow conduction to an open one that does. For other ion channels, opening produces a continuous water-filled pore, through which water and ions pass, often in single-file through the narrowest region<sup>41,42</sup>. For  $\text{H}_V1$ , channel opening produces instead a relatively dry pore that is constricted by two hydrogen bonds formed by the SF Asp and Arg<sup>14</sup> (Fig. 1a,b). Thermal fluctuations could transiently break the Asp-Arg linkage, allowing ions or water to approach the narrow SF (Fig. 1c, Figs. 2 and 3, left). The permeating  $\text{H}_3\text{O}^+$  protonates the SF Asp, resulting in favorable  $\text{AspH}^0\text{-H}_2\text{O}^0\text{-Arg}^+$  interactions (Fig. 1d), thus “opening” the pore to enable its own permeation, whereas anions ( $\text{X}^-$ ) or cations ( $\text{X}^+$ ) encounter unfavorable  $\text{Asp}^-\text{-X}^-\text{-Arg}^+$  or  $\text{Asp}^-\text{-X}^+\text{-Arg}^+$  interactions, and are ejected, restoring the Asp-Arg linkage (Fig. 2, right). Hence, the  $\text{H}_V1$  Asp-Arg SF intrinsically selects protons by virtue of its ability to “close” its pore when  $\text{H}_3\text{O}^+$  is absent, to “open” its pore by accepting a proton when  $\text{H}_3\text{O}^+$  enters, while rejecting other cations and anions through electrostatic repulsion. In the absence of permeating ions, the SF residues form hydrogen bonds that occlude the pore. Among cations,  $\text{H}_3\text{O}^+$  is uniquely able to protonate the SF ligands, permeate as neutral  $\text{H}_2\text{O}$ , and then retrieve the excess proton (Fig. 7).

The mechanism for proton selectivity found herein may also apply to other molecules. For example, if Asp112 from human  $\text{H}_V1$  is superimposed on Asp61 of the  $\text{F}_0\text{F}_1$ -type  $\text{H}^+$ -ATPase, Arg210 aligns with Arg208 of  $\text{H}_V1$  (Fig. 8). Asp61 and Arg210 are located in the proton pathway of this  $\text{H}^+$ -ATPase and are the only two amino acids that are absolutely required for function<sup>43</sup>.

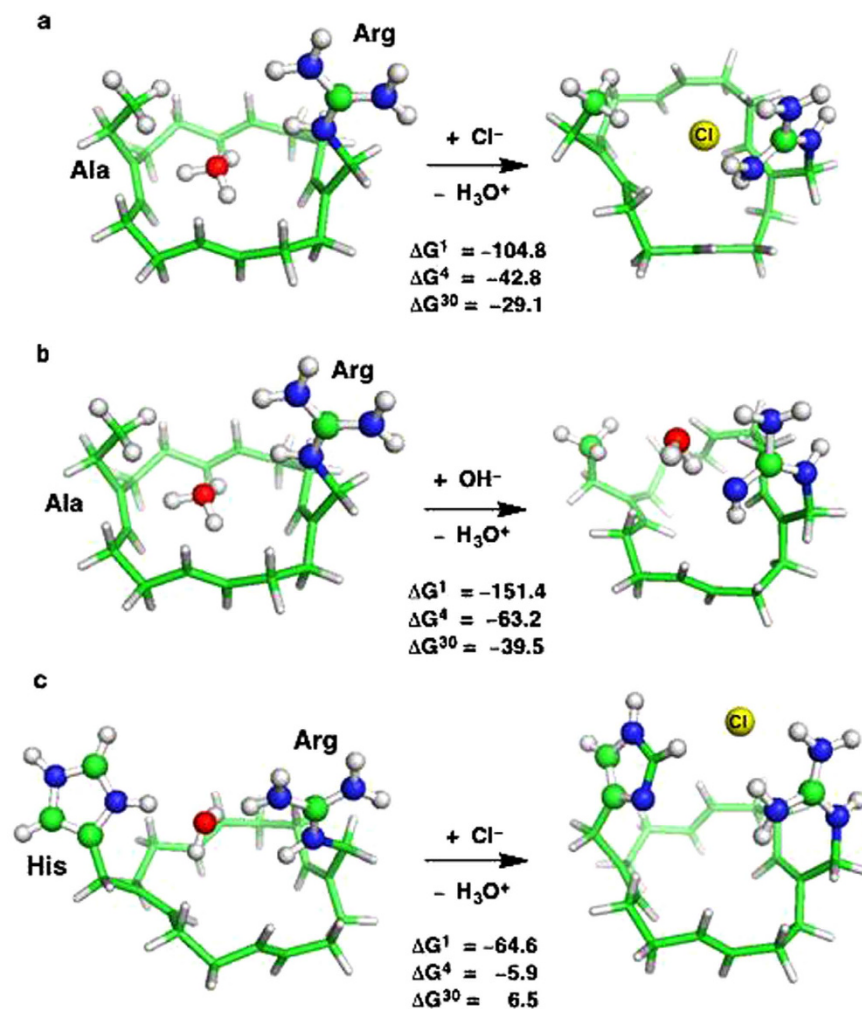


**Figure 6.** Binding of Cl<sup>-</sup> and/or OH<sup>-</sup> to H<sub>3</sub>O<sup>+</sup>-bound mutant SFs. B3LYP/6-31+G(3d,p) fully optimized structures of H<sub>3</sub>O<sup>+</sup>-SF, Cl<sup>-</sup>-SF and OH<sup>-</sup>-SF complexes, and free energies (in kcal/mol) for (a) [SF(Ala-Arg<sup>+</sup>)-H<sub>3</sub>O<sup>+</sup>] + Cl<sup>-</sup> → [SF(Ala-Arg<sup>+</sup>)-Cl<sup>-</sup>] + H<sub>3</sub>O<sup>+</sup>, (b) [SF(Ala-Arg<sup>+</sup>)-H<sub>3</sub>O<sup>+</sup>] + OH<sup>-</sup> → [SF(Ala-Arg<sup>+</sup>)-OH<sup>-</sup>] + H<sub>3</sub>O<sup>+</sup>, and (c) [SF(His-Arg<sup>+</sup>)-H<sub>3</sub>O<sup>+</sup>] + Cl<sup>-</sup> → [SF(His-Arg<sup>+</sup>)-Cl<sup>-</sup>] + H<sub>3</sub>O<sup>+</sup>.  $\Delta G^1$  is the ion exchange free energy in the gas phase, whereas  $\Delta G^4$  and  $\Delta G^{30}$  are the corresponding free energies in the SF characterized by an effective dielectric constant of 4 and 30, respectively. If the resulting free energy is negative, the pore is Cl<sup>-</sup> or OH<sup>-</sup>-selective, but if it is positive, the pore is proton-selective.

Several other proteins, which have Asp-Arg/Lys pairs thought to be critical to proton transport, also exhibit distances between the charge centers similar to the pair in H<sub>V</sub>1. Examples of such proteins and the distances between charge centers include Na<sup>+</sup> phosphatase, 3.9 Å<sup>44</sup>; H<sup>+</sup> phosphatase, 4.0 Å<sup>45</sup>; and the glucose H<sup>+</sup> symporter XylE, 4.1 Å<sup>46</sup>. In the Asp-Arg motif common to several proton pumps, a function of Arg is thought to be electrostatic ejection of the proton at the appropriate moment in the pump cycle<sup>43,47</sup>. This interacting charge pair may help enforce proton selectivity in these molecules, as in H<sub>V</sub>1.

Conversely, we searched for Asp-Arg pairs in pores of non-proton channels, where such linked acid-base pairs should not exist. We examined 60 ion channels and transporters (including various cation and anion channels, aquaporin, and organic cation transporters) for which X-ray structures exist (see Supplementary Table S6). Following criteria for a proton SF established previously<sup>19</sup>, we searched for a pore-facing Asp/Glu in hydrogen-bond contact with a single Arg/Lys, located in a narrow region of the pore in an open conformation. We found no counterexample contradicting our hypothesis.

Although the interactions between ions and the known SF ligands (notably, both amino acids directly implicated in selectivity by mutation studies) have been treated in detail using all-electron quantum mechanical calculations, the contributions from other segments of the pore and ions have not been modeled explicitly in the absence of a high-resolution structure of the open-state H<sub>V</sub>1 channel. Consequently, the present results, which are in line with experimental observations, are limited to explaining proton selectivity in the constricted, relatively dry Asp-Arg SF. How the proton leaves this SF is not explicitly dealt with here. Perhaps an incoming H<sub>3</sub>O<sup>+</sup> (or another cation) could dislodge H<sub>3</sub>O<sup>+</sup> from the SF,

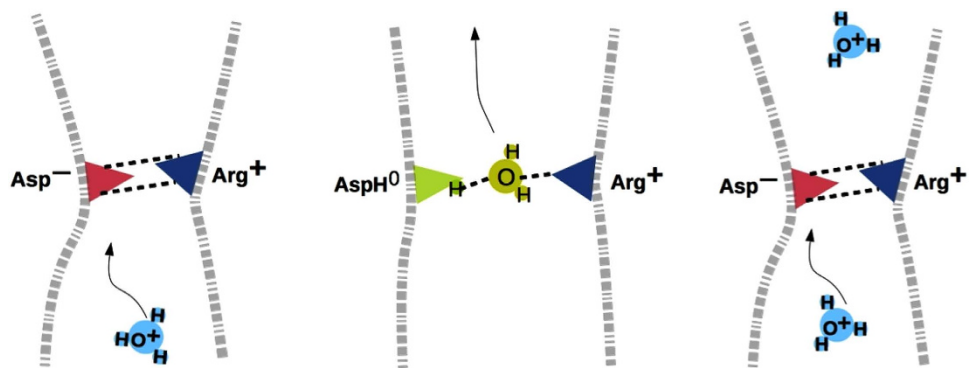


**Figure 7.** Schematic cartoon of the proposed proton selectivity mechanism by the  $H_{v1}$  SF. Negatively charged Asp is red, neutral  $AspH^0$  and  $H_2O$  are green, whereas positively charged  $H_3O^+$  and Arg are light and dark blue, respectively. The dashed lines denote hydrogen bonds or salt bridges that occlude the SF pore. When  $H_3O^+$  approaches the SF (left), it breaks the hydrogen bonds and protonates the SF, resulting in neutral  $H_2O$  bridging  $AspH^0$  and  $Arg^+$  (middle). Transfer of a proton from the SF to  $H_2O$  completes the conduction cycle (right).

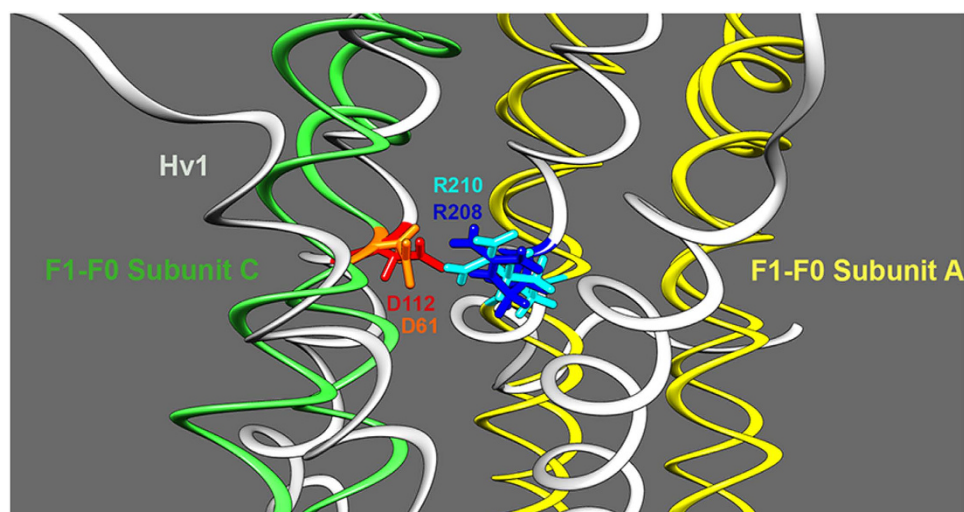


**Figure 8.** A critical Asp-Arg pair in  $F_1-F_0$  ATPase shares similar geometry to that in  $H_{v1}$ . Based on a homology model of  $H_{v1}$  in the open state<sup>14</sup> and the crystal structure of  $F_1-F_0$  ATPase (PDB ID 1C17), Asp112 in  $H_{v1}$  was superimposed onto Asp61 of  $F_1-F_0$  subunit *c* using Chimera, which minimizes the root-mean-square deviations of superimposed atoms. This resulted in Arg208 of  $H_{v1}$  occupying a similar position to Arg210 of  $F_1-F_0$  subunit *a*, which is known to participate in proton translocation.

as in the classical “knock-on” mechanism for  $K^+$  channels proposed by Hodgkin and Keynes<sup>42</sup>. MD simulations of the open  $hH_{v1}$  channel derived from multiple templates<sup>14</sup> show that the SF is located at the extracellular end of a narrow constriction  $\sim 10 \text{ \AA}$  long with a hydrophobic region surrounding Phe150–Arg211<sup>14,15</sup> at the inner end. Thus, another question is how protons pass through this second Phe150–Arg211 hydrophobic zone. However, in a recent computational study<sup>48</sup>,  $H_3O^+$  positioned at the entrance to a hydrophobic pore was found to induce water entry, creating its own water wire and lowering the free energy barrier for proton permeation. Such a mechanism may transiently hydrate the Phe–Arg bottleneck, enabling proton hopping from one water molecule to the next. When the open  $H_{v1}$  channel structure becomes available, the contributions of non-SF residues, proton coupling, and kinetic barriers to proton selectivity could be assessed from computed charge-transfer free energy profiles.

## Methods

**SF Model and Justification.** Models of the  $hH_{v1}$  SFs were built using GaussView version 3.09, following the guidelines from our previous work<sup>32</sup>. The SF ligating groups were coordinated to the permeating ion or water and attached to a carbon–hydrogen ring scaffold via flexible methylene spacers (see Figures). The ring scaffold prevents the metal ligands from drifting away or assuming unrealistic,



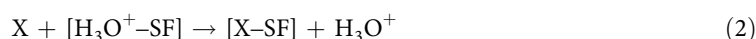
pore-occluding positions during geometry optimization. However, the shape and the C–H orientations of the ring do not obstruct the pore lumen. Moreover, the ion-ligating groups and their connection to the ring are flexible enough to allow them to optimize their positions upon ion/water binding.

**Geometry Optimization of the SF Model.** In previous studies<sup>32</sup>, the B3-LYP/6-31+G(3d,p) method was shown to be the most efficient among the various methods tested in reproducing experimentally determined molecular properties and structural characteristics of model ligands and metal complexes (see Supplementary Table S1). Hence, it was used to optimize the geometry of each model SF without any constraints and to compute the electronic energies,  $E_{el}$ , using the Gaussian 09 program. It was also used to compute the frequencies of each optimized structure. No imaginary frequency was found in any of the optimized structures.

**Free Energy Calculations.** The binding of  $H_3O^+$  to a model SF to yield  $[H_3O^+-SF]$  is described by the following reaction

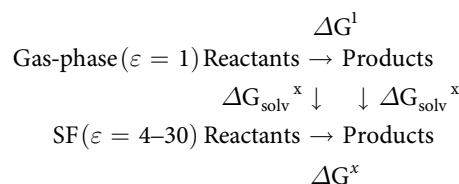


Binding of  $H_3O^+$  to the wild-type or mutant  $H_V1$  SF is thermodynamically favorable only if the binding free energy for eq 1 is negative. Following Eisenman's equilibrium theory of ion selectivity<sup>49</sup>, the filter's selectivity can be expressed in terms of the free energy  $\Delta G^x$  for replacing the native  $H_3O^+$  bound inside a model SF,  $[H_3O^+-SF]$ , with a rival ligand such as water,  $Na^+$ ,  $Cl^-$  or  $OH^-$  (denoted as X)



The native  $H_3O^+$  is preferred to the rival ligand X in the wild-type or mutant  $H_V1$  SF if  $\Delta G^x$  for eq 2 is positive or if  $\Delta G^x$  for the reverse reaction,  $[X-SF] + H_3O^+ \rightarrow X + [H_3O^+-SF]$ , is negative.  $Na^+$  or  $Cl^-$  in the SF was unstable and was found near the side chain of opposite charge in the final optimized structures, precluding determination of its binding affinity.

The reaction in eq 1 or 2 was modeled to occur in vicinity of the SF so that the dielectric environment  $\epsilon$  was assumed to be uniform for all participating entities; the respective free energy was computed using the following thermodynamic cycle:



Thus, the free energy for eq 1 or 2 can be computed as a sum of the gas-phase free energy  $\Delta G^1$  and the solvation free energy  $\Delta \Delta G_{\text{solv}}^x$  difference between the products and reactants; i.e.,

$$\Delta G^x = \Delta G^1 + \Delta \Delta G_{\text{solv}}^x \quad (3)$$

The gas-phase free energy,  $\Delta G^1$ , was computed from the electronic energy ( $\Delta E_{el}$ ), thermal energy ( $\Delta E_{th}$ ), work term ( $\Delta PV$ ), and entropy differences between products and reactants,

$$\Delta G^1 = \Delta E_{el} + \Delta E_{th} + \Delta PV - T\Delta S \quad (4)$$

The thermal energies including zero-point energy and entropies were computed from the B3-LYP/6-31+G(3d,p) frequencies scaled by an empirical factor of 0.9613<sup>50</sup>.

The solvation free energy,  $\Delta G_{\text{solv}}^x$ , was estimated by solving Poisson's equation with the MEAD program<sup>51</sup> using natural bond orbital atomic charges<sup>52</sup> and the following effective solute radii (in Å):  $R_H = 1.50$ ,  $R_H(H_3O^+) = 1.05$ ,  $R_{Na} = 1.72$ ,  $R_C = 1.95$ ,  $R_N = 1.75$ ,  $R_O(H_2O) = 1.85$ ,  $R_O(H_3O^+) = 1.65$ ,  $R_O(HO^-) = 1.64$ ,  $R_O(COO^-) = 1.56$ , and  $R_{Cl} = 2.30$ . The computed hydration free energies of the cations and ligands could reproduce the experimental values<sup>32,34,53</sup> (Supplementary Table S2).

**Validation against Experimental Free Energies.** The methodology used to compute  $\Delta G^x$  has been validated against experimental ion exchange free energies between biogenic metal cations ( $Na^+$ ,  $K^+$ , and  $Ca^{2+}$ ) in crown ethers, which resemble SF pores<sup>32</sup>, and in systems containing carboxylic ligands (nitrilotriacetic acid)<sup>34</sup>. The computed metal exchange free energies can reproduce the corresponding experimental values to within 1 kcal/mol (Supplementary Table S3)<sup>32,34,53</sup>. The methodology has yielded trends in the free energy changes that are in accord with experimental findings<sup>32-36,53-56</sup>. It has also yielded calculated pore aperture areas in good agreement with experimental estimates (Supplementary Table S4).

## References

- DeCoursey, T. E. Voltage-gated proton channels: molecular biology, physiology, and pathophysiology of the H<sub>v</sub> family. *Physiol. Rev.* **93**, 599–652, doi:10.1152/physrev.00011.2012 (2013).
- DeCoursey, T. E., Morgan, D. & Cherny, V. V. The voltage dependence of NADPH oxidase reveals why phagocytes need proton channels. *Nature* **422**, 531–534, doi:10.1038/nature01523 (2003).
- Henderson, L. M., Chappell, J. B. & Jones, O. T. G. The superoxide-generating NADPH oxidase of human neutrophils is electrogenic and associated with an H<sup>+</sup> channel. *Biochem. J.* **246**, 325–329 (1987).
- Iovannisci, D., Illek, B. & Fischer, H. Function of the HVCN1 proton channel in airway epithelia and a naturally occurring mutation, M91T. *J. Gen. Physiol.* **136**, 35–46, doi: 10.1085/jgp.200910379 (2010).
- Musset, B. *et al.* A pH-stabilizing role of voltage-gated proton channels in IgE-mediated activation of human basophils. *Proc. Natl. Acad. Sci. USA* **105**, 11020–11025, doi:10.1073/pnas.0800886105 (2008).
- Lishko, P. V., Botchkina, I. L., Fedorenko, A. & Kirichok, Y. Acid extrusion from human spermatozoa is mediated by flagellar voltage-gated proton channel. *Cell* **140**, 327–337, doi:10.1016/j.cell.2009.12.053 (2010).
- Seredenina, T., Demareux, N. & Krause, K. H. Voltage-gated proton channels as novel drug targets: From NADPH oxidase regulation to sperm biology. *Antioxid. Redox Signal in press*, doi:10.1089/ars.2013.5806 (2014).
- Wu, L. J. *et al.* The voltage-gated proton channel Hv1 enhances brain damage from ischemic stroke. *Nat. Neurosci.* **15**, 565–573, doi:10.1038/nn.3059 (2012).
- Wang, Y., Li, S. J., Wu, X., Che, Y. & Li, Q. Clinicopathological and biological significance of human voltage-gated proton channel Hv1 over-expression in breast cancer. *J. Biol. Chem.* **287**, 13877–13888, doi: 10.1074/jbc.M112.345280 (2012).
- Hondares, E. *et al.* Enhanced activation of an amino-terminally truncated isoform of the voltage-gated proton channel HVCN1 enriched in malignant B cells. *Proc. Natl. Acad. Sci. USA* **111**, 18078–18083 (2014).
- Smith, S. M. E. *et al.* Voltage-gated proton channel in a dinoflagellate. *Proc. Natl. Acad. Sci. USA* **108**, 18162–18167, doi:10.1073/pnas.1115405108 (2011).
- Taylor, A. R., Chrachri, A., Wheeler, G., Goddard, H. & Brownlee, C. A voltage-gated H<sup>+</sup> channel underlying pH homeostasis in calcifying coccolithophores. *PLoS Biol.* **9**, e1001085, doi: 10.1371/journal.pbio.1001085 (2011).
- Musset, B. *et al.* Aspartate 112 is the selectivity filter of the human voltage-gated proton channel. *Nature* **480**, 273–277, doi:10.1038/nature10557 (2011).
- Kulleperuma, K. *et al.* Construction and validation of a homology model of the human voltage-gated proton channel hHv1. *J. Gen. Physiol.* **141**, 445–465, doi:10.1085/jgp.201210856 (2013).
- Chamberlin, A., Qiu, F., Wang, Y., Noskov, S. Y. & Larsson, H. P. Mapping the gating and permeation pathways in the voltage-gated proton channel Hv1. *J. Mol. Biol.* **417**, 131–145, doi:0.1016/j.jmb.2014.11.018 (2015).
- Wood, M. L. *et al.* Water wires in atomistic models of the Hv1 proton channel. *Biochim. Biophys. Acta* **1818**, 286–293, doi:10.1016/j.bbamem.2011.07.045 (2012).
- Chamberlin, A. *et al.* Hydrophobic plug functions as a gate in voltage-gated proton channels. *Proc. Natl. Acad. Sci. U.S.A.* **111**, E273–282, doi:10.1073/pnas.1318018111 (2014).
- Li, Q. *et al.* Structural mechanism of voltage-dependent gating in an isolated voltage-sensing domain. *Nat. Struct. Mol. Biol.* **21**, 244–252 (2014).
- Morgan, D. *et al.* Peregrination of the selectivity filter delineates the pore of the human voltage-gated proton channel hHv1. *J. Gen. Physiol.* **142**, 625–640, doi:10.1085/jgp.201311045 (2013).
- DeCoursey, T. E. & Cherny, V. V. Voltage-activated hydrogen ion currents. *J. Membr. Biol.* **141**, 203–223, doi:10.1007/BF00235130 (1994).
- Takeshita, K. *et al.* X-ray crystal structure of voltage-gated proton channel. *Nat. Struct. Mol. Biol.* **21**, 352–357, doi:10.1038/nsmb.2783 (2014).
- Pupo, A., Baez-Nieto, D., Martínez, A., Latorre, R. & González, C. Proton channel models. *Channels (Austin)* **8**, 180–192, doi:10.4161/chan.28665 (2014).
- Ramsey, I. S. *et al.* An aqueous H<sup>+</sup> permeation pathway in the voltage-gated proton channel Hv1. *Nat. Struct. Mol. Biol.* **17**, 869–875, doi: 10.1038/nsmb.1826 (2010).
- Eigen, M. Proton transfer, acid-base catalysis, and enzymatic hydrolysis. Part I: elementary processes. *Angewandte Chemie, International Edition* **3**, 1–19 (1964).
- Myers, V. B. & Haydon, D. A. Ion transfer across lipid membranes in the presence of gramicidin A. II. The ion selectivity. *Biochim. Biophys. Acta* **274**, 313–322, doi: 10.1016/0005-2736(72)90179-4 (1972).
- Nagle, J. F. & Morowitz, H. J. Molecular mechanisms for proton transport in membranes. *Proc. Natl. Acad. Sci. USA* **75**, 298–302 (1978).
- Levitt, D. G., Elias, S. R. & Hautman, J. M. Number of water molecules coupled to the transport of sodium, potassium and hydrogen ions via gramicidin, nonactin or valinomycin. *Biochim. Biophys. Acta* **512**, 436–451, doi: 10.1016/0005-2736(78)90266-3 (1978).
- DeCoursey, T. E. & Hosler, J. Philosophy of voltage-gated proton channels. *J. R. Soc. Interface* **11**, 20130799, doi:10.1098/rsif.2013.0799 (2014).
- Musset, B. *et al.* Zinc inhibition of monomeric and dimeric proton channels suggests cooperative gating. *J. Physiol.* **588**, 1435–1449, doi:10.1113/jphysiol.2010.188318 (2010).
- Byerly, L., Meech, R. & Moody, W., Jr. Rapidly activating hydrogen ion currents in perfused neurones of the snail, *Lymnaea stagnalis*. *J. Physiol.* **351**, 199–216 (1984).
- DeCoursey, T. E. Voltage-gated proton channels and other proton transfer pathways. *Physiol. Rev.* **83**, 475–579, doi:10.1152/physrev.00028.2002 (2003).
- Dudev, T. & Lim, C. Determinants of K<sup>+</sup> vs. Na<sup>+</sup> selectivity in potassium channels. *J. Am. Chem. Soc.* **131**, 8092–8101 (2009).
- Dudev, T. & Lim, C. Factors governing the Na<sup>+</sup> vs. K<sup>+</sup> selectivity in sodium ion channels. *J. Am. Chem. Soc.* **132**, 2321–2332 (2010).
- Dudev, T. & Lim, C. Competition among Ca<sup>2+</sup>, Mg<sup>2+</sup>, and Na<sup>+</sup> for ion channel selectivity filters: Determinants of metal ion selectivity. *J. Phys. Chem. B* **116**, 10703–10714 (2012).
- Dudev, T. & Lim, C. Importance of metal hydration on the selectivity of Mg<sup>2+</sup> vs. Ca<sup>2+</sup> in magnesium ion channels. *J. Am. Chem. Soc.* **135**, 17200–17208, doi:10.1021/ja4087769 (2013).
- Dudev, T. & Lim, C. Evolution of eukaryotic ion channels: Principles underlying the conversion of Ca<sup>2+</sup>-selective to Na<sup>+</sup>-selective channels. *J. Am. Chem. Soc.* **136**, 3553–3559, doi:10.1021/ja4087769 (2014).
- Guillén Schlippe, Y. V. & Hedstrom, L. A twisted base? The role of arginine in enzyme-catalyzed proton abstractions. *Arch. Biochem. Biophys.* **433**, 266–278 (2005).
- Mohammed, O. F., Pines, D., Dreyer, J., Pines, E. & Nibbering, E. T. Sequential proton transfer through water bridges in acid-base reactions. *Science* **310**, 83–86, doi: 10.1126/science.1117756 (2005).
- Favre, I., Moczydlowski, E. & Schild, L. On the structural basis for ionic selectivity among Na, K and Ca in the voltage-gated sodium channel. *Biophys. J.* **71**, 3110–3125 (1996).

40. Gonzalez, C., Rebolledo, S., Perez, M. E. & Larsson, H. P. Molecular mechanism of voltage sensing in voltage-gated proton channels. *J. Gen. Physiol.* **141**, 275–285, doi:10.1085/jgp.201210857 (2013).
41. Dani, J. A. & Levitt, D. G. Water transport and ion-water interaction in the gramicidin channel. *Biophys. J.* **35**, 501–508 (1981).
42. Hodgkin, A. L. & Keynes, R. D. The potassium permeability of a giant nerve fibre. *J. Physiol.* **128**, 61–88 (1955).
43. Miller, M. J., Oldenburg, M. & Fillingame, R. H. The essential carboxyl group in subunit c of the F<sub>1</sub>F<sub>0</sub> ATP synthase can be moved and H<sup>+</sup>-translocating function retained. *Proc. Natl. Acad. Sci. USA* **87**, 4900–4904 (1990).
44. Luoto, H. H., Nordbo, E., Baykov, A. A., Lahti, R. & Malinen, A. M. Membrane Na<sup>+</sup>-pyrophosphatases can transport protons at low sodium concentrations. *J. Biol. Chem.* **288**, 35489–35499, doi:doi: 10.1074/jbc.M113.510909 (2013).
45. Lin, S. M. *et al.* Crystal structure of a membrane-embedded H<sup>+</sup>-translocating pyrophosphatase. *Nature* **484**, 399–403 (2012).
46. Sun, L. *et al.* Crystal structure of a bacterial homologue of glucose transporters GLUT1-4. *Nature* **490**, 361–366 (2012).
47. Buch-Pedersen, M. J., Pedersen, B. P., Veierskov, B., Nissen, P. & Palmgren, M. G. Protons and how they are transported by proton pumps. *Pflügers Arch.* **457**, 573–579 (2009).
48. Peng, Y., Swanson, J. M., Kang, S.-g., Zhou, R. & Voth, G. A. Hydrated excess protons can create their own water wires. *J. Phys. Chem. B*, doi:10.1021/jp5095118 (2014).
49. Eisenman, G. in *Symposium on Membrane Transport and Metabolism* (eds A. Kleinzeller & A. Kotyk) 163–179 (Academic Press 1961).
50. Wong, M. W. Vibrational frequency prediction using density functional theory. *Chem. Phys. Lett.* **256**, 391–399 (1996).
51. Bashford, D. in *Scientific Computing in Object-Oriented Parallel Environments* Vol. **1343** *Lecture Notes in Computer Science* (eds Yutaka Ishikawa, RodneyR Oldehoeft, JohnV W. Reynders, & Marydell Tholburn) Ch. **30**, 233–240 (springer Berlin Heidelberg 1997).
52. Reed, A., Weinstock, R. & Weinhold, F. Natural population analysis. *J. Chem. Phys.* **83**, 735–746 (1985).
53. Dudev, T. & Lim, C. Why voltage-gated Ca<sup>2+</sup> and bacterial Na<sup>+</sup> channels with the same EEEE motif in their selectivity filters confer opposite metal selectivity. *Phys. Chem. Chem. Phys.* **14**, 12451–12456, doi:10.1039/C2CP00036A (2012).
54. Dudev, T. & Lim, C. Bidentate vs. monodentate carboxylate coordination modes in magnesium and calcium proteins: What are the basic principles? *J. Phys. Chem. B* **108**, 4546–4557 (2004).
55. Dudev, T., Chang, L.-Y. & Lim, C. Factors governing the substitution of La<sup>3+</sup> for Ca<sup>2+</sup> and Mg<sup>2+</sup> in metalloproteins: A DFT/CDM study. *J. Am. Chem. Soc.* **127**, 4091–4103 (2005).
56. Dudev, T. & Lim, C. Competition between Li<sup>+</sup> and Mg<sup>2+</sup> in Metalloproteins. Implications for Lithium Therapy. *J. Am. Chem. Soc.* **133**, 9506–9515 (2011).

## Acknowledgments

This work was supported by Academia Sinica, MOST, Taiwan (Grant NSC-98- 2113-M-001-011), NSF MCB-1242985 (T.E.D. & S.M.E.S.), and NIH: GM102336 (T.E.D. & S.M.E.S.). T.D. is supported by the Institute of Biomedical Sciences at Academia Sinica and EU Grant “Beyond Everest”, FP7-REGPOT-2011-1.

## Author Contributions

T.D. performed the calculations. B.M., D.M., and V.C. conducted patch-clamp studies and analyzed results. S.M.E.S. provided constructs. S.M.E.S. and K.M. performed PDB data analysis. T.D., S.M.E.S. and K.M. prepared figures, T.E.D. and C.L. designed the project and discussed results. T.D., T.E.D., and C.L. participated in writing the manuscript.

## Additional Information

**Supplementary information** accompanies this paper at <http://www.nature.com/srep>

**Competing financial interests:** The authors declare no competing financial interests.

**How to cite this article:** Dudev, T. *et al.* Selectivity Mechanism of the Voltage-gated Proton Channel, H<sub>v</sub>1. *Sci. Rep.* **5**, 10320; doi: 10.1038/srep10320 (2015).



This work is licensed under a Creative Commons Attribution 4.0 International License. The images or other third party material in this article are included in the article's Creative Commons license, unless indicated otherwise in the credit line; if the material is not included under the Creative Commons license, users will need to obtain permission from the license holder to reproduce the material. To view a copy of this license, visit <http://creativecommons.org/licenses/by/4.0/>